Polymer Chemistry

A covalently crosslinked silk fibroin hydrogel using enzymatic oxidation and chemoenzymatically synthesized copolypeptide crosslinkers consisting of a GPG tripeptide motif and tyrosine: control of gelation and resilience

Journal:	*Polymer Chemistry*
Manuscript ID	PY-ART-02-2020-000187.R1
Article Type:	Paper
Date Submitted by the Author:	26-Mar-2020
Complete List of Authors:	Sogawa, Hiromitsu; RIKEN, Center of Sustainable Resource Science Katashima, Takuya; RIKEN Numata, Keiji; RIKEN,

ARTICLE

A covalently crosslinked silk fibroin hydrogel using enzymatic oxidation and chemoenzymatically synthesized copolypeptide crosslinkers consisting of a GPG tripeptide motif and tyrosine: control of gelation and resilience

Received 00th January 20xx,
Accepted 00th January 20xx

DOI: 10.1039/x0xx00000x

Hiromitsu Sogawa*[a], Takuya Katashima,[a] and Keiji Numata*[a]

A covalently crosslinked silk fibroin hydrogel (ChemSF) was successfully formed via an enzymatic crosslinking reaction using chemoenzymatically synthesized copolypeptides [poly(GPG_n-*r*-Y_m)], which consist of a glycine-proline-glycine (GPG) tripeptide motif and tyrosine (Y), as linker molecules. The gelation time of ChemSF was effectively shortened to less than 100 seconds without loss of toughness by adding poly(GPG_n-*r*-Y_m). In addition, the resilience of ChemSF was improved up to 86% at 66% strain, comparable to that of elastin, due to the flexible conformation of the poly(GPG_n-*r*-Y_m) crosslinker. The acceleration of the gelation and the improvement of the resilience of ChemSF were simultaneously achieved by using a multifunctional peptide crosslinker.

Introduction

Silk fibroin (SF) from the *Bombyx mori* (*B. mori*) silkworm is an attractive natural polymer with excellent biodegradability and biocompatibility.[1, 2] The mechanical strength and toughness of SF are attributed to the β-sheet formation of GAGAGX (X = S, Y, or A) units, which repeatedly appear in the sequence of SF.[3-6] To improve the mechanical properties of SF materials, the chemical and physical modifications of SF have been studied widely. Two reactive amino acids, serine and tyrosine, are usually utilized to modify and functionalize SF.[7, 8] For instance, a double bond capable of radical polymerization was introduced by the nucleophilic reaction of serine and 2-methacryloyloxyethyl isocyanate to give poly(methacrylate)-grafted SF,[9] whereas poly(2,6-dimethylenephenylene ether) was introduced on the side chain of SF by the oxidation coupling reaction of tyrosine and excess 2,6-dimethylphenol.[10] The conversion of tyrosine to azobenzene derivatives by diazonium coupling[11-13] and to 3,4-dihydroxyphenylalanine (DOPA) by treatment with tyrosinase[14] are other approaches to endow SF with further functionality.

One of the most-studied SF materials is the SF hydrogel.[15-19] The horseradish peroxidase (HRP)-catalyzed oxidation of tyrosine is a useful approach to generate a chemically crosslinked SF hydrogel (ChemSF) via the formation of dityrosine linkage.[20-23] For instance, SF from *B. mori* contains relatively large number of tyrosines (5.3 mol%, ~277 residues) that can participate to the crosslinking reaction.[8] Although the mechanical properties of ChemSF were lower than those of physically crosslinked SF (PhysSF) formed by intermolecular hydrogen bonds, ChemSF exhibits relatively high elasticity and resilience.[23] As these characteristics are important for its application to elastomeric and tough materials, the development of ChemSF surely contributes to achieve the new design and demand of silk-based biomaterials. In addition, not only mechanical robustness but also the control of gelation time (t_{gel}) is important for practical applications. The t_{gel} of PhysSF was tunable by changing the pH and silk concentration because the formation of a β-sheet structure is accelerated at lower pH and higher silk concentrations.[24, 25] Several additives, including glycerol and poloxamer, were also reported to shorten the t_{gel} of PhysSF.[26] In contrast, controlling the t_{gel} of ChemSF has rarely been a focus of study despite its importance.

To control resilience as well as t_{gel}, crosslinking of SF is a promising approach. We are interested in peptide-based crosslinkers to maintain the advantages of SF materials, namely, biodegradability and biocompatibility. The synthesis of peptides is still a hot topic in various fields, including drug discovery, biomedicine, and material science. Solid-phase peptide synthesis, which was developed by Merrifield,[27] is the classical method to synthesize peptides with precise sequences. However, this technique is not suitable for the large-scale production of target peptides, especially with a relatively high molecular weight. Ring-opening polymerization of amino acid *N*-carboxyanhydride (NCA) monomers is another candidate to yield polypeptides with high molecular weight and low molecular weight dispersity[28, 29] but is unsuitable for

[a] *Address here Biomacromolecules Research Team, RIKEN Center for Sustainable Resource Science, 2-1, Hirosawa, Wako-shi, Saitama, 351-0198.*
† Footnotes relating to the title and/or authors should appear here.
Electronic Supplementary Information (ESI) available: [details of any supplementary information available should be included here]. See DOI: 10.1039/x0xx00000x

sequentially controlled polymerization. The ease of tuning its sequence is important in the preparation of polypeptide-based materials for various applications. In addition, the use of phosgene or triphosgene for the synthesis of NCA monomers is unpreferable in terms of environmental load and toxin management. On the basis of the drawbacks of the existing peptide synthesis methods, chemoenzymatic polymerization of amino acid esters is attractive as an alternative environmentally benign approach for synthesizing artificial polypeptides over other conventional methods.[30-33] This biochemical polymerization can be conducted in aqueous media by producing only small byproducts, such as ethanol, and can be applied to large-scale production. With this method, Gross and coworkers reported protease-catalyzed polymerization of dipeptide monomers to give oligopeptides that have alternating sequences,[34-38] while we have developed the chemoenzymatic synthesis of artificial oligopeptides with not only linear[39-50] but also star-shaped[51, 52] and telechelic-type[53] structures. In addition, periodic sequences such as glycine-proline-glycine (GPG) tripeptide were also incorporated to improve the designability and functionality of the material.[54-56] Glycine and proline are generally key for entropic elasticity,[57, 58] and in fact, GPG analogous sequences are often found in elastomeric proteins such as elastin and resilin.[59] Moreover, the GPG sequence was also found in the major ampullate spidroin protein of spider silk and served as the flexible spacer unit between the oligoalanine domain that forms a β-sheet structure.[60, 61]

Here, we designed and synthesized peptide crosslinkers for tuning ChemSF, namely, the controls of resilience and t_{gel}. We used chemoenzymatic synthesis of copolypeptides consisting of GPG repetitive sequence and tyrosine [poly(GPG$_n$-*r*-Y$_m$)] and investigated their polymerization behavior and secondary structures. Furthermore, poly(GPG$_n$-*r*-Y$_m$) was applied to the HRP-catalyzed enzymatic crosslinking reaction of SF solutions to tune both the t_{gel} and elastic feature of ChemSF.

Experimental

Materials and measurements

Papain (product No. 164-00172), HRP (product No. 169-10791) and hydrogen peroxide (H_2O_2, 30% solution) were purchased from FUJIFILM Wako Pure Chemical Corporation (Tokyo, Japan) and used as received. The activity of papain was approximately 0.5 U/g, where one unit is defined as the amount of enzyme needed to hydrolyze 1 mmol of *N*-benzoyl-DL-arginine *p*-nitroanilide per minute at pH 7.5 and 25 °C. The activity of HPR was more than 100 U/mg. L-Tyrosine ethyl ester (Y-OEt) hydrochloride was purchased from Watanabe Chemical Industry (Hiroshima, Japan). The H-GPG-OEt tripeptide was synthesized according to the literature.[54] An SF aqueous solution was prepared according to a previously reported method.[20] Briefly, silkworm cocoons were cut into small pieces and boiled for 20 min in a 0.02 M Na_2CO_3 solution and subsequently washed with Milli-Q water. After drying for 24 h at room temperature, extracted residues were dissolved in a 9.3 M LiBr solution at 60 °C for 4 h. It was further dialyzed with Milli-Q water for 72 h using a dialysis membrane (Pierce Snake Skin MWCO 3500; Thermo Fisher Scientific, Waltham, MA, USA) to give SF aqueous solution. One milliliter of SF solution was lyophilized, and the resultant solution was weighed to determine the silk concentration. Other commercially available solvents and reagents were used as received.

^{1}H and ^{13}C nuclear magnetic resonance (NMR) spectra were recorded on a Varian NMR System 500 instrument (Varian Medical Systems, Palo Alto, CA) at 25 °C and at a frequency of 500 MHz. The mixture of dimethylsulfoxide-d_6 (DMSO-d_6) with trifluoroacetic acid-d (TFA-d) was used as the solvent for poly(GPG$_n$-*r*-Y$_m$) with tetramethylsilane as the internal standard. Matrix-assisted laser desorption/ionization time-of-flight (MALDI-TOF) mass spectrometry analysis was conducted using an ultrafleXtreme MALDI-TOF spectrophotometer (Bruker Daltonics, Billerica, MA) operating in reflectron mode at an accelerating voltage of 15 kV. The sample was dissolved in a water/acetonitrile mixture (1/1, v/v) containing 0.1% TFA and mixed with a solution of α-cyano-4-hydroxycinnamic acid (CHCA). The mixture was deposited on an MTP 384 ground steel BC target plate. Circular dichroism (CD) spectroscopic measurements were conducted using a JASCO J-820 CD spectropolarimeter (JASCO, Tokyo, Japan). A quartz cuvette with a 0.1 cm path length was used, and the scan rate was set at 100 nm/min with a bandwidth of 1 nm. Each spectrum represents the average of 10 scans from 190 to 290 nm. The contents of secondary structures were calculated by using the DichroWeb website. Attenuated total reflection Fourier transform infrared (ATR-FTIR) spectroscopy was measured on an IRPrestigae-21 Fourier transform infrared spectrophotometer (Shimadzu Corporation, Kyoto, Japan) with a MIRacle A single-reflection ATR unit using a Ge prism. The measurements were conducted from 3800 to 600 cm^{-1}, and the background spectra obtained under the same conditions were subtracted from the scan for each sample. Amino acid composition analysis was conducted using high-speed amino acid analyzers L-8900 and L8500A (Hitachi-HighTech, Tokyo, Japan).

Typical procedure for chemoenzymatic copolymerization of GPG and Y.

A solution of GPG-OEt hydrochloride (264 mg, 0.90 mmol) and Y-OEt hydrochloride (24 mg, 0.10 mmol) in phosphate buffer (PBS) (0.80 mL, 1.0 M, pH = 8.0) was placed in a glass tube equipped with a stirring bar. To this solution, 50 mg of papain in PBS (0.20 mL) was added. The final concentrations of amino acid esters and papain were 1.0 M and 50 mg/mL, respectively. The mixture was stirred at 40 °C at 800 rpm for 3 h using an EYELA ChemiStation PPS-5511 instrument (Tokyo Rikakikai Co. Ltd, Tokyo, Japan). After 3 h, the reaction mixture was cooled to room temperature, and the precipitate was collected by centrifuging at 9000 rpm and 4 °C for 20 min. It was further washed three times with Milli-Q water, centrifuged, and lyophilized to give poly(GPG$_{90}$-*r*-Y$_{10}$) as a white powder in 36% yield. The composition ratio of GPG and Y was determined by

^{1}H NMR between the integral ratio of the proline moiety of the GPG unit and the aromatic peaks of Y.

HRP-catalyzed crosslinking reaction of SF to give ChemSF

HRP was dissolved in Milli-Q water at 1000 U/mL (10 mg/mL). H_2O_2 was diluted to approximately 196 mM with Milli-Q water. Poly(GPG$_n$-*r*-Y$_m$) at several concentrations was dissolved into a 1:1 mixture of *N*-methylpyrrolidone (NMP) and PBS (0.1 M, pH 8.0). The silk solution (1 mL, 60 g/L) was mixed with poly(GPG$_n$-*r*-Y$_m$) solution (0.25 mL) and poured into a Teflon mold (15 mmϕ x 50 mm). HRP solution (45 μL) and H_2O_2 solution (20 μL) were further added and mixed by pipette to initiate the oxidation reaction. After standing for 24 h at room temperature, the cylindrical hydrogel was carefully removed from the mold and used for compression tests and FT-IR measurements soon after preparation.

Cell Culture and evaluation of cell viability

The human embryonic kidney (HEK) 293 cells (ATCC, cat. No. CRL-1573) were cultured in Dulbecco's modified Eagle's medium (DHEM) supplemented with 10% (v/v) fetal bovine serum (FBS), nonessential amino acids (0.1 mM), L-glutamine (2 mM), and 1% (v/v) penicillin–streptomycin at 37 °C in a 5% CO_2 incubator. For the evaluation of cell viability, HEK 293 cells were seeded on 96-well plates coated with ChemSF at a density of 8000 cells/well and cultured 48 h in the media (100 μL). Note that ChemSF was washed with 200 μL of D-PBS(-) for 12 h twice to remove NMP before the cell seeding. The cell viability of HEK cells on ChemSF was characterized by a standard 3-(4,5-dimethylthiazol-2-yl)-5-(3-carboxymethoxyphenyl)-2-(4-sulfophenyl)-2H-tetrazolium (MTS) assay (Promega, Madison, WI) according to the manufacturer's instructions (n = 6). The cell viability was calculated as follows:
[cell viability,%] = [absorbance at 490 nm of the cell culture incubated on ChemSF in the presence of peptide crosslinkers] / [absorbance at 490 nm of the cell culture incubated on ChemSF in the absence of peptide crosslinker] x 100

Rheological measurements during the HRP-catalyzed crosslinking reaction

To an SF aqueous solution (1 mL, 60 g/L), poly(GPG$_n$-*r*-Y$_m$) in NMP/PBS = 1/1 (0.25 mL), HRP solution (45 μL) and H_2O_2 (20 μL) were added. Then, the reaction mixture was set between the cone and plate fixtures of a rheometer. The diameter and angles of the cone fixture were 50 mm and 4°, respectively. The storage elastic modulus (*G*′) and the loss elastic modulus (*G*″) during the oxidation reaction were measured using a stress-controlled rheometer (MCR 102 Anton Paar, Austria). The experiments were conducted 3 times for every condition. The temperature was set to 25 °C. The strain and frequency were 10% and 10 Hz, respectively. Prior to the measurement, we confirmed that the applied strain was within the range of the linear viscoelasticity.

Compression tests

Compression tests were conducted by a mechanical testing apparatus (EZ-Test, Shimadzu, Kyoto, Japan) with a compression rate of 10 mm/min. The obtained stress-strain relationships corresponded to the equilibrium relationships without time effects because no appreciable relaxation in stress was observed after imposing constant strain at this crosshead speed. The measurements were performed at a relative humidity of approximately 40% and a temperature of 25 °C. The Young's modulus (*E*), strain at break, compressive strength, and fracture energy were analyzed based on the stress-strain curves of the prepared samples. The experiments were conducted at least 5 times for every condition. Cycle tests were also conducted with a loading and unloading rate of 10 mm/min. The resilience at each strain was calculated by the following equation:

$$\text{Resilience (\%)} = A_2/A_1 \times 100 \quad (1)$$

where A_2 and A_1 are the total areas under the unloading and loading curves, respectively.[62, 63]

Statistical analysis

The significance of differences in the studies of mechanical properties was determined by unpaired t-tests with a two-tailed distribution, whereas those of cell viability was analyzed by one-way ANOVA with Tukey's multiple test.

Results and discussion

Chemoenzymatic copolymerization of GPG and Y

The chemoenzymatic polymerization was conducted using papain as a catalyst in PBS (1.0 M, pH 8.0) at 40 °C by changing the feed ratio of GPG and Y monomers to give poly(GPG$_n$-*r*-Y$_m$) as a white precipitate. This precipitate was washed with Milli-Q water and collected by centrifugation. The results are summarized in Table 1. The isolated yields of poly(GPG$_n$-*r*-Y$_m$) decreased upon adding equal amounts of GPG and Y. In particular, the insoluble part was not detected at a feed ratio of 60/40 (Table 1, run 5). As the formation of short oligopeptides was confirmed in the soluble part by MALDI-TOF MS, the solubility of the formed poly(GPG$_{60}$-*r*-Y$_{40}$) was higher than that of others, resulting in a decrease in the yield. To increase the yields, we further attempted the copolymerization in cases of the feed ratio of 80/20, 60/40, and 40/60 by changing the total monomer concentrations ([M]$_{total}$) to 0.5 and 2.0 M, which are half and twice of the initial one (Table S1). Besides, the papain concentration was also doubled from 50 to 100 mg/mL. As results, the yield improved by increasing the papain concentration in case of the feed ratio of 80/20 (Table S1, runs 3 vs 4) and 60/40 (runs 8 vs 9). Notably, the precipitate of poly(GPG$_{60}$-*r*-Y$_{40}$) appeared at 4% yield although no precipitate was formed at the initial condition. On the other hands, the decrease of the total monomer concentration was effective for a feed ratio of 40/60 (runs 14 vs 15). This is because Y monomer can be polymerized more efficiently at the monomer concentration of ca. 0.5 M.[64] We also considered to apply other enzymes such as bromelain and proteinase K. Bromelain is a cysteine protease, that is same as papain, whereas proteinase K is a serine one. These

two enzyme was used for the homopolymerization of GPG, however, papain gave better results in terms of yields and molecular weights of formed polymer (Table S2). Thus, we did not further apply them to the copolymerization. In short, the significant improvement of yields of copolymerization was still difficult due to the several reasons such as the solubility increase of formed copolypeptides due to the increase of randomness of their sequences, and affinity differences of GPG and Y monomers for the enzyme. To overcome this issue, further trials are needed to find out the suitable polymerization conditions and enzymes to obtain copolypeptides, whose molecular weights are high enough to precipitate from reaction media. The composition ratio of the two monomers was determined by the integral ratio of proline peaks of the GPG monomer (c and d) and aromatic peaks of the Y monomer (i and j) in the ^{1}H NMR spectra (Figures 1 and S1). The linear relationship between the feeding and composition ratio was confirmed at high GPG contents (Table 1, runs 1–4), while it was lost when the Y monomer was abundant (runs 7–10). This result is probably due to the difference in propagation rates of the two monomers and the low solubility of tyrosine-rich peptides. Poly(GPG$_{100}$) and poly(Y$_{100}$) exhibited a series of peaks in the MALDI-TOF MS spectra whose intervals corresponded to the molar masses of the GPG tripeptide and Y unit, respectively (Figure S2). The molecular weight of poly(GPG$_{100}$) was in the range of 1,000–2,800 g/mol, whereas that of poly(Y$_{100}$) was approximately 1,000. Poly(GPG$_{100}$) possessed a higher molecular weight due to both its high affinity for papain and its high solubility in PBS. As obvious from the peak molecular weights (M_p) in Table 1, this trend was also observed for the copolypeptides; for example, the peaks of poly(GPG$_{80}$-*r*-Y$_{20}$) appeared in the higher molecular weight region compared to those of poly(GPG$_{40}$-*r*-Y$_{60}$) and poly(GPG$_{20}$-*r*-Y$_{80}$) (Figure 2). In addition, peaks attributed to repetitive GPG units and zero or one tyrosine were observed for poly(GPG$_{80}$-*r*-Y$_{20}$), whereas poly(GPG$_{40}$-*r*-Y$_{60}$) and poly(GPG$_{20}$-*r*-Y$_{80}$) contained tyrosine-rich sequences without showing repetitive peaks of homopolytyrosine.

Table 1. Chemoenzymatic copolymerization of GPG and Y

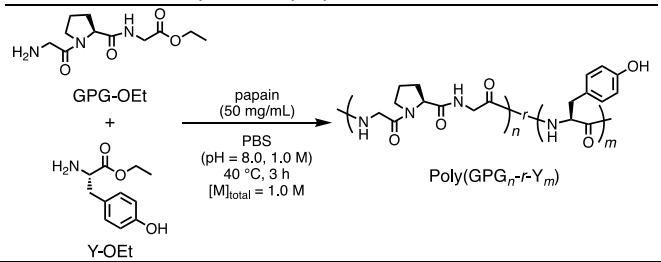

run	monomer ratio (%) GPG	Y	code	yield (%)[a]	M_p[b]	composition ratio (%)[c] GPG	Y
1	100	0	Poly(GPG$_{100}$)	40	1300	100	–
2	90	10	Poly(GPG$_{80}$-*r*-Y$_{10}$)	36	1300	94	6
3	80	20	Poly(GPG$_{80}$-*r*-Y$_{20}$)	11	1300	90	10
4	75	25	Poly(GPG$_{75}$-*r*-Y$_{25}$)	12	1700	86	14
5	60	40	Poly(GPG$_{60}$-*r*-Y$_{40}$)	–[c]	–[d]	–[d]	–[d]
6	50	50	Poly(GPG$_{50}$-*r*-Y$_{50}$)	5	1300	52	48
7	40	60	Poly(GPG$_{40}$-*r*-Y$_{60}$)	15	1300	29	71
8	25	75	Poly(GPG$_{25}$-*r*-Y$_{75}$)	33	1100	15	85
9	20	80	Poly(GPG$_{20}$-*r*-Y$_{80}$)	37	1100	12	88
10	10	90	Poly(GPG$_{10}$-*r*-Y$_{90}$)	48	1100	12	88
11[e]	0	100	Poly(Y$_{100}$)	41	1100	–	100

[a]H_2O-insoluble part. [b]Detected by MALDI-TOF MS. [c]Measured by ^{1}H NMR. [c]No precipitate. [d]Not determined. [e][Y] = 0.6 M.

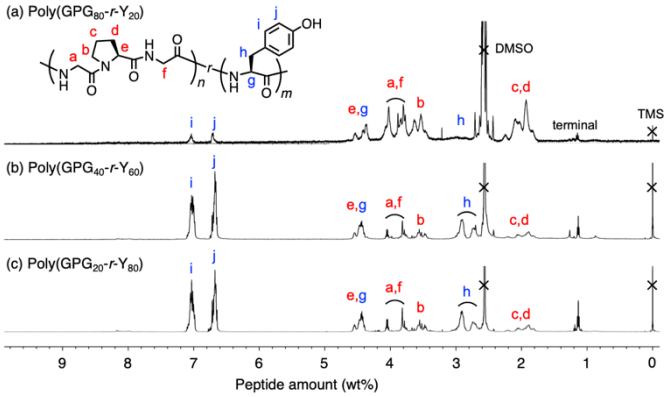

Figure 1. ^{1}H NMR spectra of (a) poly(GPG$_{80}$-*r*-Y$_{20}$), (b) poly(GPG$_{40}$-*r*-Y$_{60}$), and (c) poly(GPG$_{20}$-*r*-Y$_{80}$). [500 MHz, DMSO-d$_6$/TFA-d = 5/1 (v/v)].

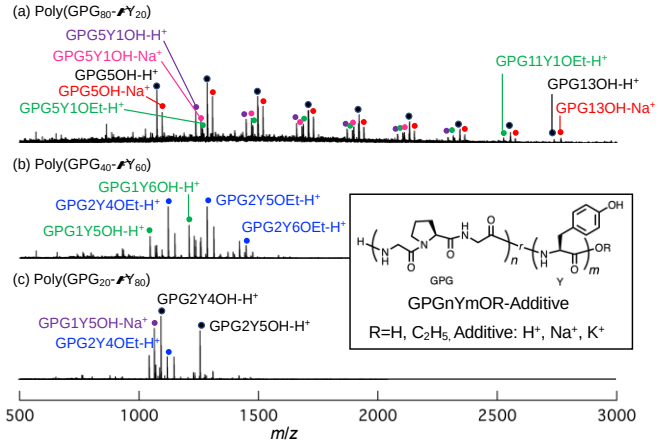

Figure 2. MALDI-TOF MS of (a) poly(GPG$_{80}$-*r*-Y$_{20}$), (b) poly(GPG$_{40}$-*r*-Y$_{60}$), and (c) poly(GPG$_{20}$-*r*-Y$_{80}$). Matrix: CHCA, mode: reflectron positive. The peaks were assigned with the codes "GPGnYmOR-Additive", where n, m, R, and Additive represent the repeating number of GPG unit, that of Y unit, *C*-terminal structure (H or Et), and adducted cation (H^+ or Na^+ or K^+), respectively. For a detailed assignments of peaks, see ESI (Figure S2).

Secondary structures of poly(GPG$_n$-*r*-Y$_m$)

Prior to the preparation of ChemSF, the secondary structure of poly(GPG$_n$-*r*-Y$_m$) was evaluated by CD spectroscopy (Figure S3). 2,2,2-Trifuloreethanol (TFE) was used as a solvent because poly(GPG$_n$-*r*-Y$_m$) did not dissolve in water. The contents of the secondary structures were calculated using the DichroWeb online CD analysis server (Figure S4 and Table S3). Poly(GPG$_{100}$) exhibited positive and negative peaks at 205 and 190 nm, respectively. Poly(GPG$_n$-*r*-Y$_m$) in which *m* is greater than 50

showed an additional positive peak centered at 225 nm, attributed to the aromatic absorption region of the tyrosine residue. CD analysis revealed that the β-strand was the dominant structure for all the obtained peptides. For example, poly(GPG$_{80}$-*r*-Y$_{20}$), poly(GPG$_{40}$-*r*-Y$_{60}$), and poly(GPG$_{20}$-*r*-Y$_{80}$) accounted for 38%, 46% and 43% of the β-strand structure at 20 °C, respectively. This result was also supported by FT-IR measurements, as poly(GPG$_n$-*r*-Y$_m$) showed amide I absorption peaks at 1650 cm^{-1}, which were attributed to the β-sheet structure (Figure S5). It should also be noted that the content of the β-turn structure was larger for GPG-rich copolypeptides (β-turn: 26–28%) than for Y-rich copolypeptides (19–24%), probably because the bent conformation of the proline units enhanced the adoption of the turn structure, similar to spider silk proteins in the amorphous sequence.[65] Additionally, a significant reversible change in peak shape was observed upon heating and cooling. The content of the β-strand decreased at the evaluated temperature, and those of the β-turn and unordered structures increased instead. Poly(GPG$_n$-*r*-Y$_m$) showed a structural transition similar to that of short elastin and resilin-like peptides.[66, 67]

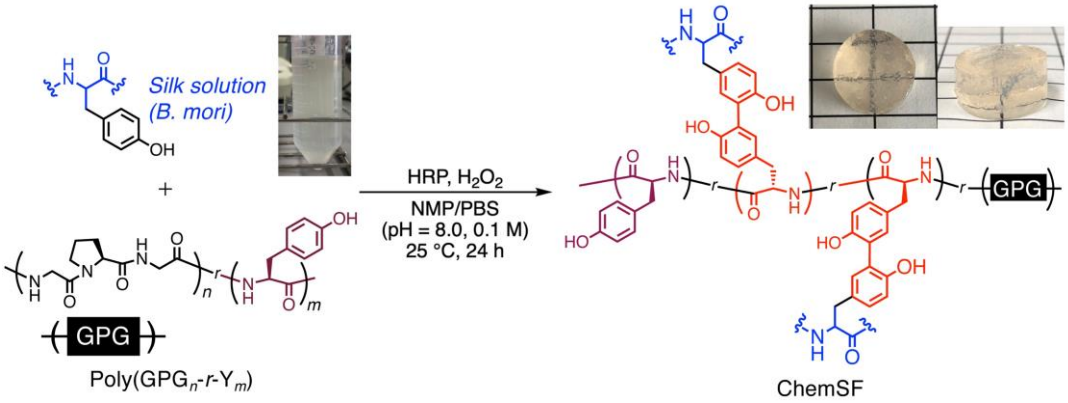

Scheme 1. HRP-catalyzed enzymatic crosslinking reaction of SF solutions using a poly(GPG$_n$-*r*-Y$_m$) crosslinker.

Enzymatic crosslinking reaction to afford ChemSF with a poly(GPG$_n$-*r*-Y$_m$) crosslinker

We then examined the enzymatic crosslinking reaction of SF using poly(GPG$_n$-*r*-Y$_m$) as a crosslinker. Poly(GPG$_{80}$-*r*-Y$_{20}$), poly(GPG$_{40}$-*r*-Y$_{60}$), and poly(GPG$_{20}$-*r*-Y$_{80}$) were applied to the reaction in this study, and their amounts were varied in the range of 0.06 to 0.38 wt%. As shown in Scheme 1, the treatment of SF solution (60 g/L) and poly(GPG$_n$-*r*-Y$_m$) with HRP and H$_2$O$_2$ at 25 °C gave transparent and elastic ChemSF. Note that this reaction proceeded smoothly even in the presence of a small amount of organic solvent (NMP). To evaluate the gelation kinetics for each condition, dynamic time-dependent *G*′ and *G*″ were monitored using a rheometer. As shown in Figure S6, *G*′ rapidly increased and became higher than *G*″, suggesting that the reaction mixture was changed from the sol state to the gel state. The crossover point of *G*′ and *G*″ is set as t_{gel} and summarized in Figure 3. Obviously, t_{gel} was effectively shortened by increasing the amount and Y content of the poly(GPG$_n$-*r*-Y$_m$) crosslinker. *G*′ was larger than *G*″ within 100 seconds after mixing 0.38 wt% of poly(GPG$_{20}$-*r*-Y$_{80}$), indicating that t_{gel} was shorter than our observation time under this condition. In other words, t_{gel} was shortened to less than half of the original value upon adding only a small portion of poly(GPG$_{20}$-*r*-Y$_{80}$). Poly(GPG$_{80}$-*r*-Y$_{20}$) was not as effective in terms of shortening the t_{gel} because it contained only zero or one Y unit in the single peptide chain although at least two or more Y units were required to be the effective crosslinker, as suggested by MALDI-TOF measurements (Figures 2a and S2c).

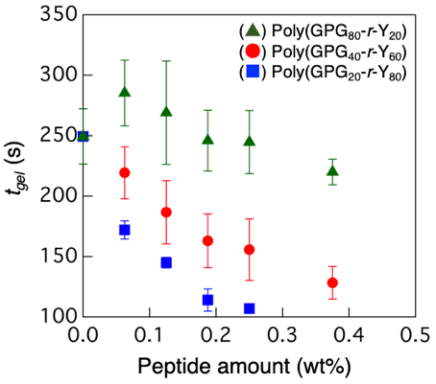

Figure 3. The t_{gel} of ChemSF using a poly(GPG$_n$-*r*-Y$_m$) crosslinker.

Further experiments on the feeding of poly(GPG$_n$-*r*-Y$_m$) above 0.38 wt% were not conducted due to the difficulty of observing t_{gel} under this condition.

To gain knowledge about the network structure of ChemSF, the efficiency of the enzymatic crosslinking reaction was evaluated by amino acid analysis (Figure S7). ChemSF samples that had been washed with Milli-Q water several times were analyzed by the ninhydrin method.[68] An SF solution was also analyzed as the unreacted control sample. As summarized in Table S4, the content of Y significantly decreased after the enzymatic reaction, although those of other amino acids remained unchanged. The conversion ratio of Y was calculated as 30% by adding 1.0 wt% poly(GPG$_{40}$-*r*-Y$_{60}$) to SF solution. Note that we could not distinguish the Y residues of either SF or poly(GPG$_n$-*r*-Y$_m$) that were converted. In addition, a significant increase in P was not observed even after the addition of poly(GPG$_n$-*r*-Y$_m$) because its amount was too small and negligible compared to that of SF. Furthermore, the HRP-

catalyzed model oxidation reaction of Boc-Y-OH was also conducted (Figure S8). In the ^{1}H NMR spectra, characteristic aromatic peaks corresponding to the dityrosine structure were confirmed after treating Boc-Y-OH under the same conditions as the ChemSF preparation.[69] The conversion ratio was estimated to be 31%, which was coincident with the result of amino acid analysis. These results suggested that ChemSF formed a covalently crosslinked network structure via dityrosine linkages, leaving various contents of unreacted tyrosine residues, as shown in Scheme 1. The absence of physical crosslinking points was confirmed by FT-IR measurements. Namely, the formed ChemSF displayed amide I absorption at 1640 cm^{-1} or higher wavenumber regions (Figure S9), indicating that the SF scaffold adopted a random conformation as a major structure.[70]

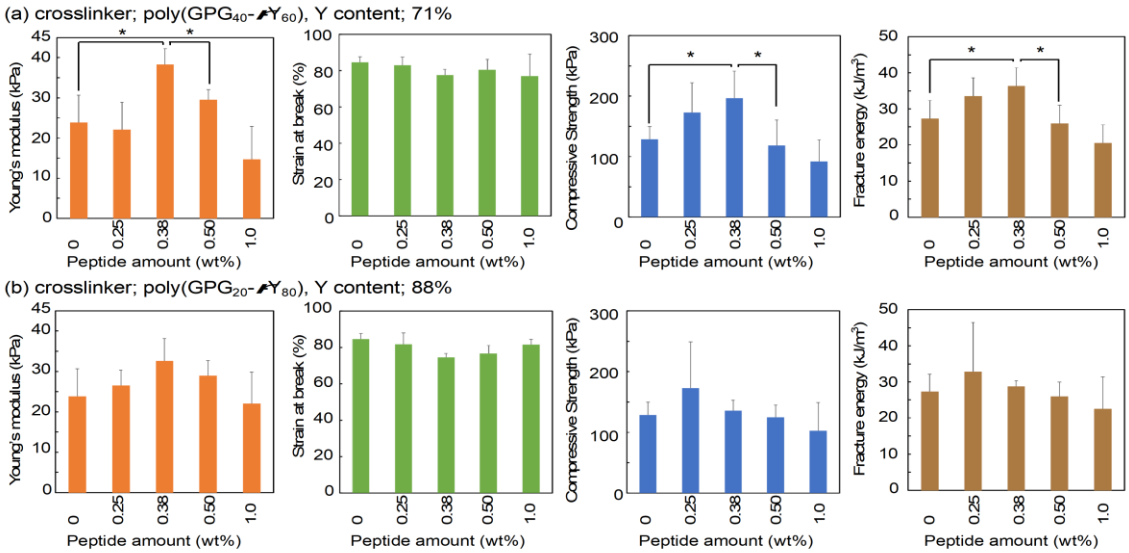

Figure 4. Mechanical properties including the Young's modulus, strain at break, compressive strength, and fracture energy of ChemSF obtained by using (a) poly(GPG$_{40}$-*r*-Y$_{60}$) and (b) poly(GPG$_{20}$-*r*-Y$_{80}$). *Significant differences between groups at $p < 0.1$.

Next, the mechanical properties of ChemSF were evaluated by compression tests to clarify whether the difference in t_{gel} affects its toughness or not (Figure S10). As poly(GPG$_{80}$-*r*-Y$_{20}$) did not effectively accelerate gelation, the ChemSF samples obtained by using poly(GPG$_{40}$-*r*-Y$_{60}$) and poly(GPG$_{20}$-*r*-Y$_{80}$) crosslinkers were tested by compressing the samples at 10 mm/min. Figure 4 summarizes the mechanical properties, including the Young's modulus (E), strain at break, compressive strength, and fracture energy. As a result, the E of ChemSF was approximately 20–50 kPa, which was similar to the previous report by Partlow *et al.*[23] It increased significantly by increasing the amount of poly(GPG$_{40}$-*r*-Y$_{60}$) and reached a maximum at 0.38 wt%, while a further increase had a negative influence. Notably, this value was even lower than that of the original ChemSF, which was obtained without adding poly(GPG$_n$-*r*-Y$_m$). To discuss this point in more detail, the theoretical prediction of the phantom network model, which is one of the major molecular models to describe the rubber elasticity of chemically crosslinked hydrogels, was considered. This model assumes that the crosslinking points can fluctuate and that the deformation of the network strands is suppressed by the fluctuation. In this model, E can be described by the following equation:

$$E = 3(\nu - \mu)k_{B}T \quad (2)^{71, 72}$$

where ν, μ, k_B, and T are the number density of the network strands, that of the crosslinks, Boltzmann constant, and absolute temperature, respectively. In this study, a four-functional junction point, which has two network strands, is formed by assuming that the crosslinking reaction occurs ideally. Then, ν and μ are described as follows:

$$\nu = 2(C_{crosslinker}/m_{crosslinker}) \quad (3a)$$
$$\mu = C_{crosslinker}/m_{crosslinker} \quad (3b)$$

where $C_{crosslinker}$ and $m_{crosslinker}$ are the concentration and molar mass of poly(GPG$_n$-*r*-Y$_m$), respectively. In this study, $m_{crosslinker}$ of poly(GPG$_{40}$-*r*-Y$_{60}$) and poly(GPG$_{20}$-*r*-Y$_{80}$) was determined as 178 and 170 g/mol respectively, based on the average molecular weights of their repeating units. As ChemSF possesses chemical crosslinking by HRP even in the absence of poly(GPG$_n$-*r*-Y$_m$), equation (2) is modified as follows:

$$E = 3(\nu - \mu)k_{B}T + E_{original} \quad (4)$$

where $E_{original}$ was experimentally estimated to be 27.3 kPa by compression tests of ChemSF sample, which was prepared in the absence of poly(GPG$_n$-*r*-Y$_m$). By substituting equation (3a) and (3b) into (4), equation (4) can be rewritten as follows.

$$E = 3[2(C_{crosslinker}/m_{crosslinker}) - (C_{crosslinker}/m_{crosslinker})]k_BT + E_{original}$$
$$= 3k_BTC_{crosslinker}/m_{crosslinker} + E_{original} \quad (5)$$

The simulated E was represented as the solid line in Figure 5 based on Equation (5). The model prediction was in good agreement with the experimental values in the low crosslinker

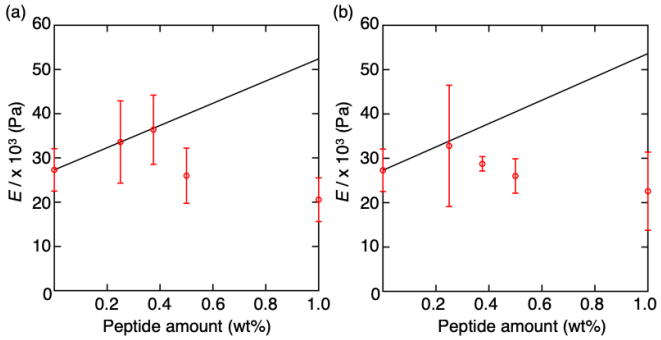

Figure 5. Relationships between E and peptide amount for (a) poly(GPG$_{40}$-*r*-Y$_{60}$) and (b) poly(GPG$_{20}$-*r*-Y$_{80}$). The red-colored data points with error bars were measured values by compression tests. The black solid line was estimated by equation (5). $m_{crosslinker}$ of poly(GPG$_{40}$-*r*-Y$_{60}$) and poly(GPG$_{20}$-*r*-Y$_{80}$) was determined as 178 and 170 g/mol, respectively. $E_{original}$ was experimentally estimated to be 27.3 kPa. T = 298 K, k_B = 1.38 x 10^{-23} JK^{-1}.

concentration region (~0.38 wt%), suggesting that the crosslinking points were introduced effectively by the addition of poly(GPG$_{40}$-*r*-Y$_{60}$) in this range. On the other hand, in the high crosslinking concentration region above 0.50 wt%, E was lower than the prediction, which suggests that the excess amount of poly(GPG$_{40}$-*r*-Y$_{60}$) prevented effective crosslinking formation (Figure 5a). The excessive acceleration of t_{gel} by adding a lot of peptide crosslinkers might enhance the formation of inhomogeneous network structure. A similar tendency was observed for poly(GPG$_{20}$-*r*-Y$_{80}$). It seems that the E value reached the maximum by adding a lower amount of poly(GPG$_{20}$-*r*-Y$_{80}$) than of poly(GPG$_{40}$-*r*-Y$_{60}$) (Figure 4b). In addition, disagreement with the prediction model was observed in the lower range (Figure 5b) because the increase in the Y ratio led to the enhancement of the hydrophobicity of poly(GPG$_n$-*r*-Y$_m$). This enhancement induced the aggregation of the poly(GPG$_n$-*r*-Y$_m$) crosslinker in aqueous-rich medium, which inhibited the formation of ideal network structures. It could be concluded that poly(GPG$_n$-*r*-Y$_m$) contributed to the formation of the dense network structure and improved the toughness of ChemSF, at least in the range in which the acceleration of t_{gel} was observed (0 to 0.38 wt%).

Meanwhile, cycle tests were performed to evaluate the resilience of ChemSF. As mentioned above, the introduction of a flexible GPG sequence has the potential to improve the resilience of ChemSF. Typical loading-unloading compressive tests were performed for ChemSF at 10 mm/min. As shown in Figure S11, ChemSF showed negligible energy loss, unlike PhysSF, especially over a small strain range, indicating the absence of a change in the network structures at this deformation range. Figure 6 summarizes the resilience percentages of ChemSF using poly(GPG$_{40}$-*r*-Y$_{60}$) at different strains, whose values were calculated by equation (1).[62, 63] The resilience values of ChemSF with 0.5 and 1 wt% poly(GPG$_{40}$-*r*-Y$_{60}$) were omitted in Figure 6, as the theoretical model prediction implied that poly(GPG$_{40}$-*r*-Y$_{60}$) was not incorporated into the network structure effectively at these weight amounts.

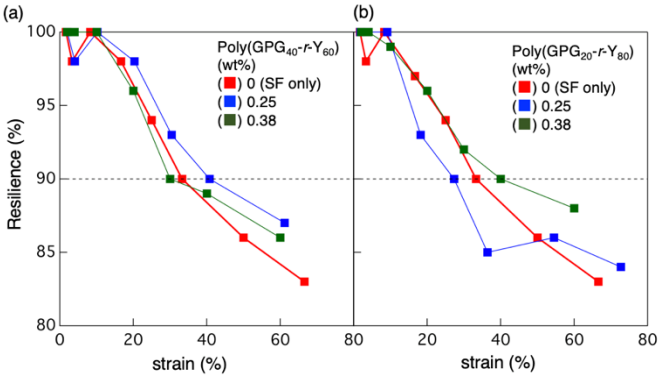

Figure 6. Resilience of ChemSF obtained by using (a) poly(GPG$_{40}$-*r*-Y$_{60}$) and (b) poly(GPG$_{20}$-*r*-Y$_{80}$).

ChemSF with 0 to 0.38 wt% poly(GPG$_{40}$-*r*-Y$_{60}$) showed comparable resilience to elastin in the small to medium strain range (<40%),[66, 73] whereas 80% resilience remained even in the larger strain range (>40%). Slight improvement of the resilience was observed by the addition of poly(GPG$_{40}$-*r*-Y$_{60}$), especially at a larger strain range. For instance, ChemSF in the absence of poly(GPG$_{40}$-*r*-Y$_{60}$) showed 83% resilience at 66% strain (red line in Figure 6), while it was increased to 87% at 61% strain and 86% at 60% strain by adding 0.25 wt% and 0.38 wt% of poly(GPG$_{40}$-*r*-Y$_{60}$), respectively (blue and green line). Similar improvement was observed for poly(GPG$_{20}$-*r*-Y$_{80}$) (Figure 6b), indicating that the flexible GPG sequence in poly(GPG$_n$-*r*-Y$_m$) was assumed to contribute to enhancing the elastic properties of ChemSF.

Finally, we evaluated the cell viability of ChemSF using an MTS assay. A cell viability of 100% was calculated from the cell culture seeded on ChemSF in the absence of peptide crosslinker after incubation for 48 h as a control. Then, the obtained data was analyzed by one-way ANOVA with Tukey's multiple

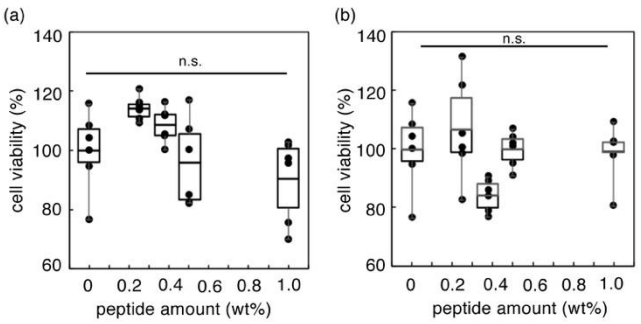

Figure 7. Cell viability of HEK cells seeded on ChemSF in the presence of (a) poly(GPG_{40}-*r*-Y_{60}) and (b) poly(GPG_{20}-*r*-Y_{80}). It was determined from the absorbance at 490 nm measured using the cell cultures after incubation for 48 h. A cell viability of 100% was calculated from a control, namely, the cell culture seeded on ChemSF in the absence of peptide crosslinkers. The horizonal line in the box plot represents the average value and the box is drawn from 25% to 75% quartiles (n = 6). A one-way ANOVA was performed with Tukey's multiple comparison test to compare the values in each pair. N.s. indicates the samples are not significantly different at $p < 0.01$.

comparison test to compare the values in each pair. As results, there was no significant difference at $p < 0.01$ between the samples. All ChemSF samples showed similar cell viability and no clear trend depending on the amount and composition of peptide crosslinkers was observed in the measuring range. Further increase of peptide crosslinker might show negative effects for the cell viability because the slope of the approximate straight line was negative, however, we did not conduct above 1wt% crosslinker condition in terms of mechanical toughness. Briefly, gradual decrease of mechanical toughness of ChemSF was suggested by compression tests with the addition of above this amount of peptide crosslinkers.

Conclusions

Chemoenzymatic copolymerization of the GPG tripeptide and Y was successfully achieved to give random copolypeptides [poly(GPG_n-*r*-Y_m)]. The structures of the formed poly(GPG_n-*r*-Y_m) were fully characterized by NMR, MALDI-TOF, CD analysis and FT-IR measurements. Covalently crosslinked SF hydrogels, ChemSFs, were prepared via an HRP-catalyzed reaction using synthesized poly(GPG_n-*r*-Y_m) as a crosslinker. Both the acceleration of gelation and the improvement of resilience of ChemSF were simultaneously achieved with the use of poly(GPG_n-*r*-Y_m). The knowledge obtained in this study is expected to contribute to the development of practical elastic silk materials in the biomedical and bioengineering fields.

Conflicts of interest

The authors declare no conflicts of interest.

Acknowledgments

This work was financially supported by the Impulsing Paradigm Change through Disruptive Technologies Program (ImPACT) of the Japan Science and Technology Corporation (JST), Japan Society for the Promotion of Science (JSPS) KAKENHI Grant Number 19K15644, the RIKEN Engineering Network, and JST ERATO (Grant Number JPMJER1602). We also thank the Support Unit for Bio-Material Analysis, RIKEN CBS Research Resources Division, for technical help with amino acid analysis.

Notes and references

1. C. Holland, K. Numata, J. Rnjak-Kovacina and F. P. Seib, *Adv. Healthc. Mater.*, 2019, **8**, e1800465.
2. L.-D. Koh, Y. Cheng, C.-P. Teng, Y.-W. Khin, X.-J. Loh, S.-Y. Tee, M. Low, E. Ye, H.-D. Yu and Y.-W. Zhang, *Prog. Polym. Sci.*, 2015, **46**, 86-110.
3. A. D. Malay, R. Sato, K. Yazawa, H. Watanabe, N. Ifuku, H. Masunaga, T. Hikima, J. Guan, B. B. Mandal, S. Damrongsakkul and K. Numata, *Sci. Rep.*, 2016, **6**, 27573.
4. C. Fu, Z. Shao and V. Fritz, *Chem. Commun.*, 2009, DOI: 10.1039/B911049F, 6515-6529.
5. H.-J. Jin and D. L. Kaplan, *Nature*, 2003, **424**, 1057.
6. C. Z. Zhou, F. Confalonieri, M. Jacquet, R. Perasso, Z. G. Li and J. Janin, *Proteins: Structure, Function, and Bioinformatics*, 2001, **44**, 119-122.
7. T. Katashima, A. D. Malay and K. Numata, *Curr. Opin. Chem. Eng.*, 2019, **24**, 61-68.
8. A. R. Murphy and D. L. Kaplan, *J. Mater. Chem.*, 2009, **19**, 6443-6450.
9. T. Furuzono, K. Ishihara, N. Nakabayashi and Y. Tamada, *Biomaterials*, 2000, **21**, 327-333.
10. L. Simmons, K. Tsuchiya and K. Numata, *RSC Adv.*, 2016, **6**, 28737-28744.
11. Z. Wang, C. Li, H. Zhang and Z. Liu, *Fibers and Polymers*, 2018, **19**, 2134-2138.
12. L. Raynal, B. J. Allardyce, X. Wang, R. J. Dilley, R. Rajkhowa and L. C. Henderson, *J. Mater. Chem. B*, 2018, **6**, 8037-8042.
13. A. R. Murphy, P. S. John and D. L. Kaplan, *Biomaterials*, 2008, **29**, 2829-2838.
14. H. Sogawa, N. Ifuku and K. Numata, *ACS Biomater. Sci. Eng.*, 2019, **5**, 5644–5651.
15. A. M. Hopkins, L. De Laporte, F. Tortelli, E. Spedden, C. Staii, T. J. Atherton, J. A. Hubbell and D. L. Kaplan, *Adv. Funct. Mater.*, 2013, **23**, 5140-5149.
16. U. J. Kim, J. Y. Park, C. M. Li, H. J. Jin, R. Valluzzi and D. L. Kaplan, *Biomacromolecules*, 2004, **5**, 786-792.
17. K. Numata, T. Katashima and T. Sakai, *Biomacromolecules*, 2011, **12**, 2137-2144.
18. K. Numata, S. Yamazaki and N. Naga, *Biomacromolecules*, 2012, **13**, 1383-1389.
19. A. Matsumoto, J. Chen, A. L. Collette, U. J. Kim, G. H. Altman, P. Cebe and D. L. Kaplan, *J. Phys. Chem. B*, 2006, **110**, 21630-21638.
20. K. Numata, N. Ifuku, H. Masunaga, T. Hikima and T. Sakai, *Biomacromolecules*, 2017, **18**, 1937-1946.
21. T. V. Chirila, S. Suzuki and C. Papolla, *Biotechnol. Appl. Biochem.*, 2017, **64**, 771-781.
22. M. McGill, J. M. Coburn, B. P. Partlow, X. Mu and D. L. Kaplan, *Acta biomaterialia*, 2017, **63**, 76-84.
23. B. P. Partlow, C. W. Hanna, J. Rnjak - Kovacina, J. E. Moreau, M. B. Applegate, K. A. Burke, B. Marelli, A. N. Mitropoulos, F. G. Omenetto and D. L. Kaplan, *Adv. Funct. Mater.*, 2014, **24**, 4615-4624.
24. S. Nagarkar, T. Nicolai, C. Chassenieux and A. Lele, *PCCP*, 2010, **12**, 3834-3844.
25. T. Hanawa, A. Watanabe, T. Tsuchiya, R. Ikoma, M. Hidaka and M. Sugihara, *Chem. Pharm. Bull.* 1995, **43**, 284-288.
26. G. D. Kang, J. H. Nahm, J. S. Park, J. Y. Moon, C. S. Cho and J. H. Yeo, *Macromol. Rapid Commun.*, 2000, **21**, 788-791.
27. B. Merrifield, *Science*, 1986, **232**, 341-347.
28. C. Deng, J. Wu, R. Cheng, F. Meng, H.-A. Klok and Z. Zhong, *Prog. Polym. Sci.*, 2014, **39**, 330-364.

29. J. Huang and A. Heise, *Chem. Soc. Rev.*, 2013, **42**, 7373-7390.
30. K. Tsuchiya and K. Numata, *Macromol. Biosci.*, 2017, **17**, 1700177.
31. S.-i. Shoda, H. Uyama, J.-i. Kadokawa, S. Kimura and S. Kobayashi, *Chem. Rev.*, 2016, **116**, 2307-2413.
32. K. Yazawa and K. Numata, *Molecules*, 2014, **19**, 13755-13774.
33. S. Kobayashi and A. Makino, *Chem. Rev.*, 2009, **109**, 5288-5353.
34. G. Li, J. Wu, X. Qin, J. Zhu, K. Viswanathan, H. Dong, P. Somasundaran and R. A. Gross, *Langmuir*, 2014, **30**, 6889-6896.
35. X. Qin, A. C. Khuong, Z. Yu, W. Du, J. Decatur and R. A. Gross, *Chem. Commun.*, 2013, **49**, 385-387.
36. X. Qin, W. Xie, S. Tian, J. Cai, H. Yuan, Z. Yu, G. L. Butterfoss, A. C. Khuong and R. A. Gross, *Chem. Commun.*, 2013, **49**, 4839-4841.
37. G. Li, V. K. Raman, W. Xie and R. A. Gross, *Macromolecules*, 2008, **41**, 7003-7012.
38. G. Li, A. Vaidya, K. Viswanathan, J. Cui, W. Xie, W. Gao and R. A. Gross, *Macromolecules*, 2006, **39**, 7915-7921.
39. T. Miyamoto, K. Tsuchiya and K. Numata, *Biomacromolecules*, 2019, **20**, 653-661.
40. K. Tsuchiya and K. Numata, *ACS Macro Lett.*, 2017, **6**, 103-106.
41. Y. Ma, R. Sato, Z. Li and K. Numata, *Macromol. Biosci.*, 2016, **16**, 151-159.
42. S. Nitta, A. Komatsu, T. Ishii, H. Iwamoto and K. Numata, *Polym. J.*, 2016, **48**, 955.
43. J. M. Ageitos, K. Yazawa, A. Tateishi, K. Tsuchiya and K. Numata, *Biomacromolecules*, 2015, **17**, 314-323.
44. K. Numata, *Polym. J.*, 2015, **47**, 537.
45. P. J. Baker, S. V. Patwardhan and K. Numata, *Macromo. Biosci.*, 2014, **14**, 1619-1626.
46. J. Fagerland, A. Finne-Wistrand and K. Numata, *Biomacromolecules*, 2014, **15**, 735-743.
47. K. Numata and P. J. Baker, *Biomacromolecules*, 2014, **15**, 3206-3212.
48. P. J. Baker and K. Numata, *Biomacromolecules*, 2012, **13**, 947-951.
49. K. Yazawa and K. Numata, *Polymers*, 2016, **8**, 194.
50. K. Yazawa, J. Gimenez-Dejoz, H. Masunaga, T. Hikima and K. Numata, *Polym. Chem.*, 2017, **8**, 4172-4176.
51. J. M. Ageitos, J. A. Chuah and K. Numata, *Macromol. Biosci.*, 2015, **15**, 990-1003.
52. J. M. Ageitos, P. J. Baker, M. Sugahara and K. Numata, *Biomacromolecules*, 2013, **14**, 3635-3642.
53. K. Tsuchiya and K. Numata, *Macromol. Biosci.*, 2016, **16**, 1001-1008.
54. P. G. Gudeangadi, K. Tsuchiya, T. Sakai and K. Numata, *Polym. Chem.*, 2018, **9**, 2336-2344.
55. K. Tsuchiya and K. Numata, *Chem. Commun.*, 2017, **53**, 7318-7321.
56. K. Tsuchiya and K. Numata, in *Green Polymer Chemistry: New Products, Processes, and Applications*, American Chemical Society, 2018, vol. 1310, ch. 7, pp. 95-105.
57. S. Cheng, M. Cetinkaya and F. Gräter, *Biophys. J.*, 2010, **99**, 3863-3869.
58. S. Rauscher, S. Baud, M. Miao, Fred W. Keeley and R. Pomès, *Structure*, 2006, **14**, 1667-1676.
59. L. Li, M. B. Charati and K. L. Kiick, *Polym. Chem.*, 2010, **1**, 1160-1170.
60. A. D. Malay, K. Arakawa and K. Numata, *PLOS ONE*, 2017, **12**, e0183397.
61. G. B. Perea, C. Riekel, G. V. Guinea, R. Madurga, R. Daza, M. Burghammer, C. Hayashi, M. Elices, G. R. Plaza and J. Pérez-Rigueiro, *Sci. Rep.*, 2013, **3**, 3061.
62. J. Cui, M. A. Lackey, A. E. Madkour, E. M. Saffer, D. M. Griffin, S. R. Bhatia, A. J. Crosby and G. N. Tew, *Biomacromolecules*, 2012, **13**, 584-588.
63. Z. Zha, W. Teng, V. Markle, Z. Dai and X. Wu, *Biopolymers*, 2012, **97**, 1026-1036.
64. H. Uyama, T. Fukuoka, I. Komatsu, T. Watanabe and S. Kobayashi, *Biomacromolecules*, 2002, **3**, 318-323.
65. Sandeep P. Patil, B. Markert and F. Gräter, *Biophys. J.*, 2014, **106**, 2511-2518.
66. M. B. Charati, J. L. Ifkovits, J. A. Burdick, J. G. Linhardt and K. L. Kiick, *Soft Matter*, 2009, **5**, 3412-3416.
67. M. Cao, Y. Shen, Y. Wang, X. Wang and D. Li, *Molecules*, 2019, **24**.
68. S. Moore and W. H. Stein, *J. Biol. Chem.*, 1948, **176**, 367-388.
69. D.-I. Lee, J.-Y. Choi, C.-J. Kim and I.-S. Ahn, *Process Biochem.*, 2011, **46**, 142-147.
70. X. Hu, D. Kaplan and P. Cebe, *Macromolecules*, 2006, **39**, 6161-6170.
71. H. M. James and E. Guth, *J. Chem. Phys.*, 1953, **21**, 1039-1049.
72. M. Rubinstein and R. H. Colby, *Polymer physics*, Oxford university press New York, 2003.
73. L. Li, S. Teller, R. J. Clifton, X. Jia and K. L. Kiick, *Biomacromolecules*, 2011, **12**, 2302-2310.

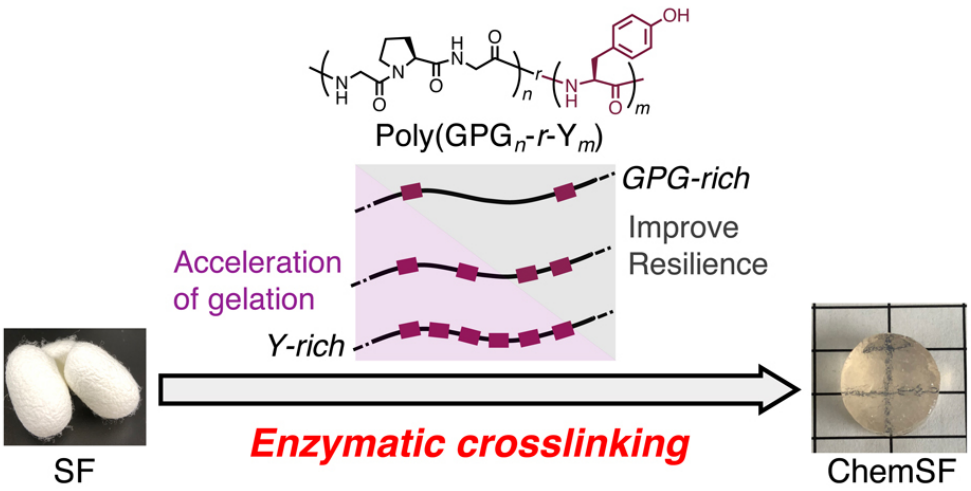

80x39mm (300 x 300 DPI)